Surface Inclusion of Unidirectional Molecular Motors in Hexagonal Tris(o-phenylene)cyclotriphosphazene

Kaleta, Jiri; Chen, Jiawen; Bastien, Guillaume; Dracinsky, Martin; Masat, Milan; Rogers, Charles T.; Feringa, Ben L.; Michl, Josef

Published in:
Journal of the American Chemical Society

DOI:
10.1021/jacs.7b05404

Publication date:
2017

JACS
JOURNAL OF THE AMERICAN CHEMICAL SOCIETY
Article
pubs.acs.org/JACS

Surface Inclusion of Unidirectional Molecular Motors in Hexagonal Tris(*o*-phenylene)cyclotriphosphazene

Jiří Kaleta,*[,†] Jiawen Chen,[‡] Guillaume Bastien,[†] Martin Dračínský,[†] Milan Mašát,[†] Charles T. Rogers,[§] Ben L. Feringa,*[,‡] and Josef Michl[†,∥]

[†]Institute of Organic Chemistry and Biochemistry AS CR, Flemingovo nám. 2, 166 10 Praha 6, Czech Republic

[‡]Department of Organic and Molecular Inorganic Chemistry, Stratingh Institute, University of Groningen, Nijenborgh 4, 9747 AG Groningen, The Netherlands

[§]Department of Physics, University of Colorado, Boulder, Colorado 80309, United States

[∥]Department of Chemistry and Biochemistry, University of Colorado, Boulder, Colorado 80309, United States

Supporting Information

ABSTRACT: A new unidirectional light-driven molecular motor suitable for host–guest surface inclusion complexes with tris(*o*-phenylene)cyclotriphosphazene (TPP) was synthesized. The motor molecules formed regular two-dimensional trigonal arrays covering the large facets of disc-shaped TPP nanocrystals. Photochemical and thermal isomerization studies demonstrated that the light-driven rotation of the anchored motors is similar to that observed in solution and is not compromised neither by either the surface confinement or the density of surface coverage (50 vs 100%).

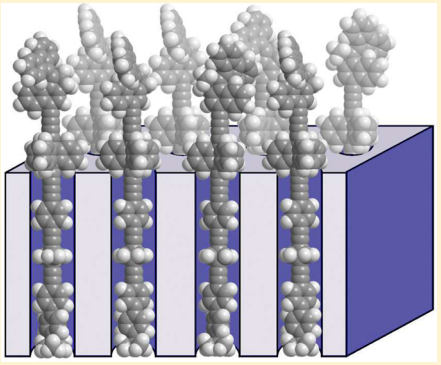

INTRODUCTION

The ability to control molecular motion at the nanoscale is the basis for dynamic molecular systems and molecular machines that ultimately will enable complex tasks akin to the functioning of motor proteins in the living cell.[1−9] Taking inspiration both from macroscopic machines and biological motors, a large variety of artificial rotors[10] and motors[11] have been designed in order to study and/or exploit rotary and translational movement of their molecular components. These range from biaryls[12] and metal-(ball-bearing) complexes,[13] surface mounted-,[14,15] crystalline-[16,17] and geared-[18] rotors, rotaxane shuttles[19] and catenane rotors[20] to light-driven[21] and chemically powered[22−24] molecular motors and machines based on the dynamics of covalent, coordinative and mechanical bonds. The understanding of the elementary features and operational mechanisms of rotors and motors has stimulated the construction of more sophisticated functional dynamic systems, including transporters,[25−27] autonomous molecular machines,[28,29] synthesizers,[30] and of applications ranging from information storage[31,32] to responsive materials.[33−35]

Among the major challenges ahead in the rapidly emerging field of molecular machines are the precise positioning and collective behavior of molecular rotors and motors that will allow the synchronization and amplification of their motion.[6] Recent studies have taken advantage of surface mounted motors,[36−39] metallo-organic frameworks,[40,41] gels,[42] polymers[43] and liquid crystals,[44−46] but surface assembly, with nanoscale precision in positioning rotary motors, would represent a major step toward two-dimensional arrays of motors.

Here we report the surface inclusion and light-driven rotary motion of arrays of unidirectional molecular motors in hexagonal tris(*o*-phenylene)cyclotriphosphazene (TPP), building on prior experience with these materials.[47−49] The synthesis of a second generation rotary motor with a long shaft, which allows its inclusion as guest in the nanochannels of the TPP host, is presented along with the formation of nanoscale facets of disc shaped TPP crystals covered with rotary motors. Extensive solid state NMR, UV–vis and powder X-ray diffraction confirm the formation of surface inclusion complexes. Photochemical and thermal isomerization studies demonstrate that the rotation of the motors is not compromised by the surface confinement.

The design of the target host–guest system showing molecular motors assembled on a facet of a TPP crystal is shown in Figure 1. Here advantage is taken of the long-known[50−53] tendency of long rod shaped molecules to include in the hexagonal channels of TPP. Molecular motors are mounted on top of the shafts and upon surface assembly precise 2D positioning is achieved due to the ∼1.1 nm spacing

Received: May 25, 2017
Published: June 27, 2017

DOI: 10.1021/jacs.7b05404
J. Am. Chem. Soc. 2017, 139, 10486−10498

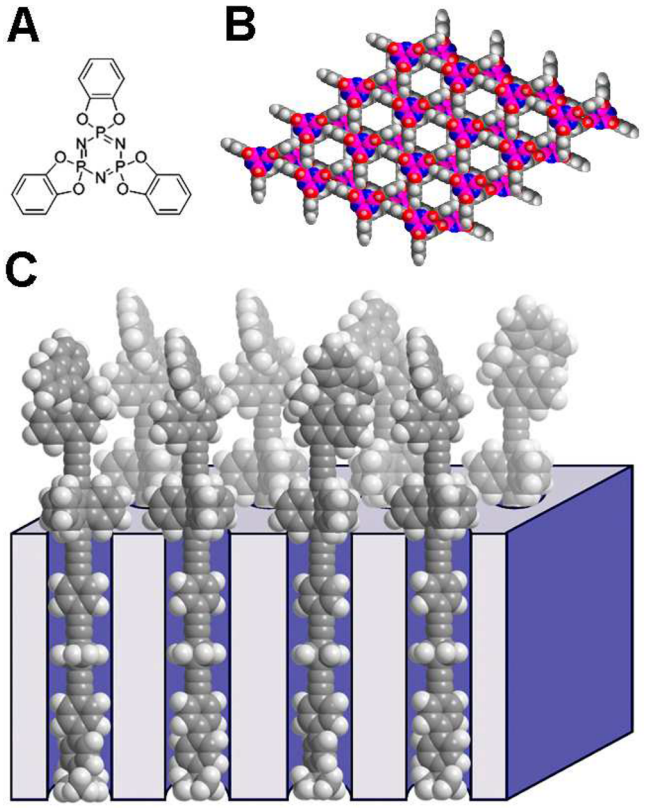

Figure 1. Chemical formula of TPP (A), top view of two successive layers of hexagonal TPP (B), and an idealized model of molecular motors mounted on a facet of TPP crystal (C).

of the TPP channels, which allows sufficient room for the rotor components of the motor to operate.

Structure **1** (Chart 1) is based on a previously developed concept:[49] a long nonpolar shaft (a) suitable for insertion into a TPP channel is connected to a triptycene stopper (b) too bulky to enter. The stopper carries a linker (c) with a molecular motor located above the surface and consisting of an indene-like stator (d) and a rotating fluorene-based rotator (e). The whole immersed part of the molecular rotor **1** may rotate within the TPP channel.

The *long shaft* (a) serves two main purposes. (i) It firmly anchors the entire structure into a TPP channel through van der Waals interactions with the interior of the channel,[48,54] and (ii) it allows a monitoring of the depth of insertion by providing two ^{13}C NMR markers (a *tert*-butyl group located at the shaft end and a bicyclo[1.1.1]penta-1,3-diyl unit, abbreviated as BCP, placed near the shaft center) whose resonances do not overlap with other motor signals.

The *triptycene stopper* (b), whose equatorial diameter is ~9.2 Å, has already proven its ability to prevent complete insertion of the entire molecule into a TPP channel[49] (internal diameter,[55] 4.5−5.0 Å).

The *linker* (c). The use of butadiyne instead of acetylene is synthetically more convenient, since the former is much more reactive in Sonogashira cross-coupling reactions.[56] It is also less likely to introduce a rotational barrier for the rotator motion. A disadvantage is its greater flexibility.

The *stator* (d) and the *rotator* (e) are based on previous work on light-driven molecular motors.[57]

Chart 1. Unidirectional Light-Driven Molecular Motor 1s Built from a Shaft (a), a Triptycene Stopper (b), a Linker (c), a Stator (d), and a Rotor (e)[a]

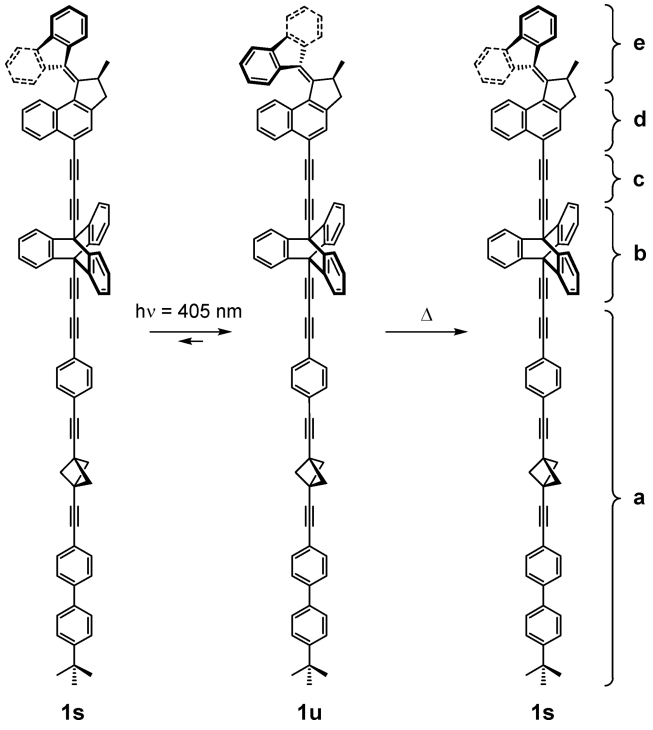

[a]A single enantiomer is depicted.

RESULTS

We describe a synthesis of the light-driven molecular motor **1s** and prove its thermal helix inversion in solution using two independent methods, ^{1}H nuclear magnetic resonance (NMR) and ultraviolet absorption spectroscopy (UV−vis). We examine the formation of surface inclusions using two different guest loadings (5 and 10 mol %), and characterize them by solid-state nuclear magnetic resonance (ssNMR), powder X-ray diffraction (XRD), transmission electron microscopy (TEM), and differential scanning calorimetry (DSC). Finally, the ability of these surface-mounted molecular motors to undergo unidirectional rotational motion is documented by time-dependent UV−vis spectroscopy. We characterize the thermal step in the light-induced intramolecular rotation for **1s** both in solution and in surface inclusion by determining its enthalpy ($\Delta H^{\ddagger}$) and Gibbs free energy ($\Delta G^{\ddagger}$) of activation.

Synthesis. The synthetic approach to **1** utilizes a previously published[49] modular strategy based on the preparation of two fairly soluble building blocks (molecular motor carrying triptycene stopper **2** and bicyclo[1.1.1]pentane-based shaft **3**), whose subsequent Sonogashira coupling yields the poorly soluble and easily isolated target compound.

The functional heart of **1**, the alkene **4**, is accessible from 1-bromonaphthalene (**5**) in four synthetic steps (Scheme 1). Condensation of **5** with methacrylic acid in polyphosphoric acid (PPA) at 110 °C gave ketone **6**,[58] which was converted to thioketone **7** by stirring with Lawesson's reagent. The unstable **7** was immediately treated with diazofluorenone (**8**)[57] to afford the bromoalkene **9** in an overall yield of 21% after two steps. Subsequent aromatic Finkelstein reaction converted **9** to the more reactive iodo derivative **4** in 90% yield (Scheme 1).

DOI: 10.1021/jacs.7b05404
J. Am. Chem. Soc. 2017, 139, 10486−10498

Scheme 1. Preparation of the Iodide 4

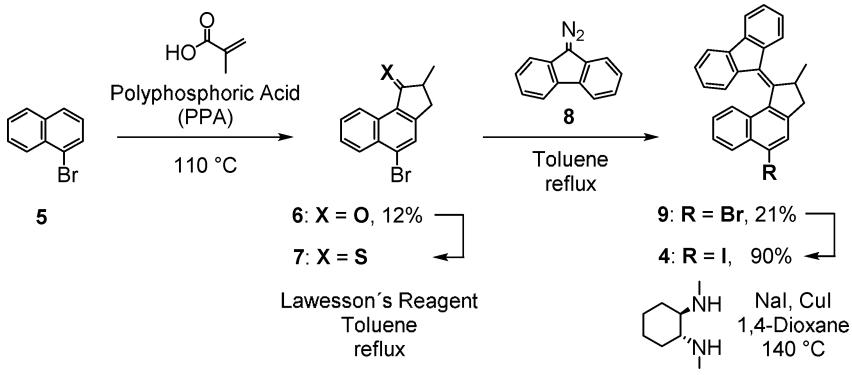

The Sonogashira coupling between **4** and **10** gave the silyl derivative **11** in high yield (Scheme 2). The free terminal

Scheme 2. Final Assembly of the Molecular Motor 1

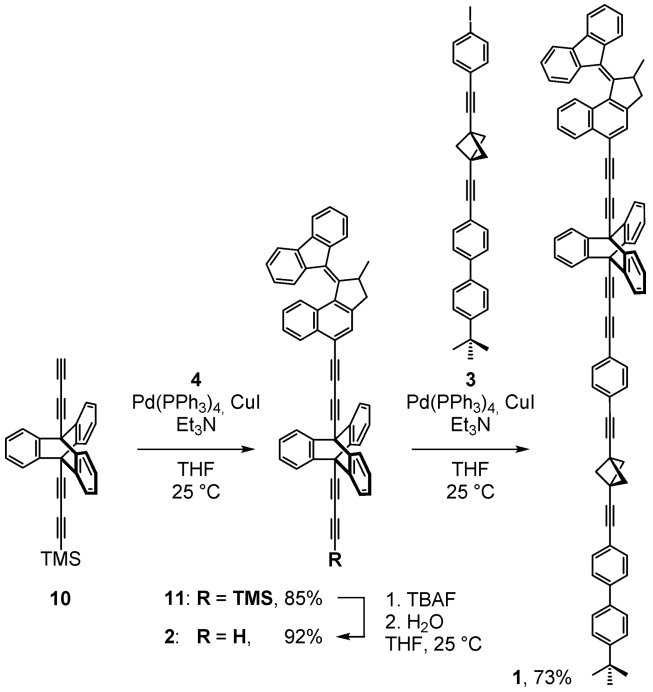

alkyne **2** was then liberated from **11** using TBAF in THF. Final Sonogashira coupling of the alkyne **2** with the iodo derivative **3** resulted in quantitative (based on the ^{1}H NMR of the crude reaction mixture) formation of the molecular motor **1**, which precipitated from the reaction mixture. Isolation and purification reduced the isolated yield to 73% (Scheme 2), similar to yields previously reported for structurally related molecular rotors.[49]

Solution ^{1}H and ^{13}C NMR Spectra of 1. Since the NMR technique is essential for detection of light-induced isomerization of **1s** in solution and for characterization of surface inclusions, all ^{1}H and most ^{13}C resonances (except for six triple bond carbon signals) were assigned (Figure 2) using ^{1}H-^{1}H correlation spectroscopy (COSY), ^{13}C attached-proton test (APT), heteronuclear single quantum coherence (HSQC), and heteronuclear multiple bond correlation (HMBC). Only a few characteristic ^{1}H and ^{13}C resonances were assigned in the stator and rotor parts (d and e, Chart 1) of **1u** (Figure 2), because all other aromatic signals were overlapped with peaks of **1s**.

Preparation and Characterization of Surface Inclusions. Freshly synthesized hexagonal solvent-free TPP-d_{12} and an appropriate amount of **1s** were mixed, ball-milled at room temperature, and annealed at 70 °C to obtain 5%**1s**@TPP-d_{12}, and 10%**1s**@TPP-d_{12} (10% corresponds to the estimated maximum surface saturation, cf. Supporting Information, Page S2).

Solid-State ^{13}C and ^{31}P NMR. ^{13}C cross-polarization magic-angle spinning (CP MAS) was used for neat **1s** and both inclusion compounds, which were also examined by ^{31}P CP MAS and ^{31}P single pulse excitation (SPE). The nearly fully assigned ^{13}C resonances of **1s** in solution (Figure 2) provide a background for understanding the solid-state NMR spectra of both neat **1s** and of inclusions 5%**1s**@TPP-d_{12}, and 10%**1s**@TPP-d_{12}.

The solid-state ^{13}C CP MAS NMR spectrum of **1s** (Figure 3B) shows a similar peak pattern as the ^{13}C solution spectrum, but some peaks are slightly shifted. Most of the aromatic carbon resonances are well resolved in solution NMR (Figure 3A), but are overlapped in solid-state NMR and appear as five broad and featureless peaks in the region 110−150 ppm in the ^{13}C CP MAS NMR (Figure 3B). The solid-state NMR spectra of both samples, 5%**1s**@TPP-d_{12} and 10%**1s**@TPP-d_{12}, are almost identical and similar to that of neat **1s**, but some peaks are shifted (Figure 3C,D). In addition, both spectra also contain three additional peaks in the aromatic region, due to the three inequivalent carbon signals of hexagonal TPP.

Because of the complex structure of **1s** only a few mostly aliphatic carbon signals were useful for the characterization of inclusion complexes. Five characteristic ^{13}C resonances originating in the nonpolar shaft (a, Chart 1) of **1s** in $CDCl_3$ solution are shown in orange and purple in Figure 3A. The green and black peaks correspond to characteristic carbon signals of the triptycene unit, the motor section, and some triple bonds.

The terminal *tert*-butyl group has two easily identifiable signals with chemical shifts 31.3 ppm (CH_3 groups) and 34.6 ppm (quaternary carbon atom) in $CDCl_3$ solution and 31.9 ppm and 34.8 ppm in ^{13}C CP MAS NMR of neat **1s** (orange peaks). Both of these signals are shifted upfield in 5%**1s**@TPP-d_{12} (30.9 and 33.6 ppm) and 10%**1s**@TPP-d_{12} (30.9 and 33.9 ppm) (Figure 3).

In solution the central bicyclo[1.1.1]pentane cage has three characteristic signals: two chemically inequivalent bridgehead carbon atoms at 30.8 and 31.1 ppm, and three equivalent methylene bridge carbons at 59.1 ppm. The signals of the two

DOI: 10.1021/jacs.7b05404
J. Am. Chem. Soc. 2017, 139, 10486−10498

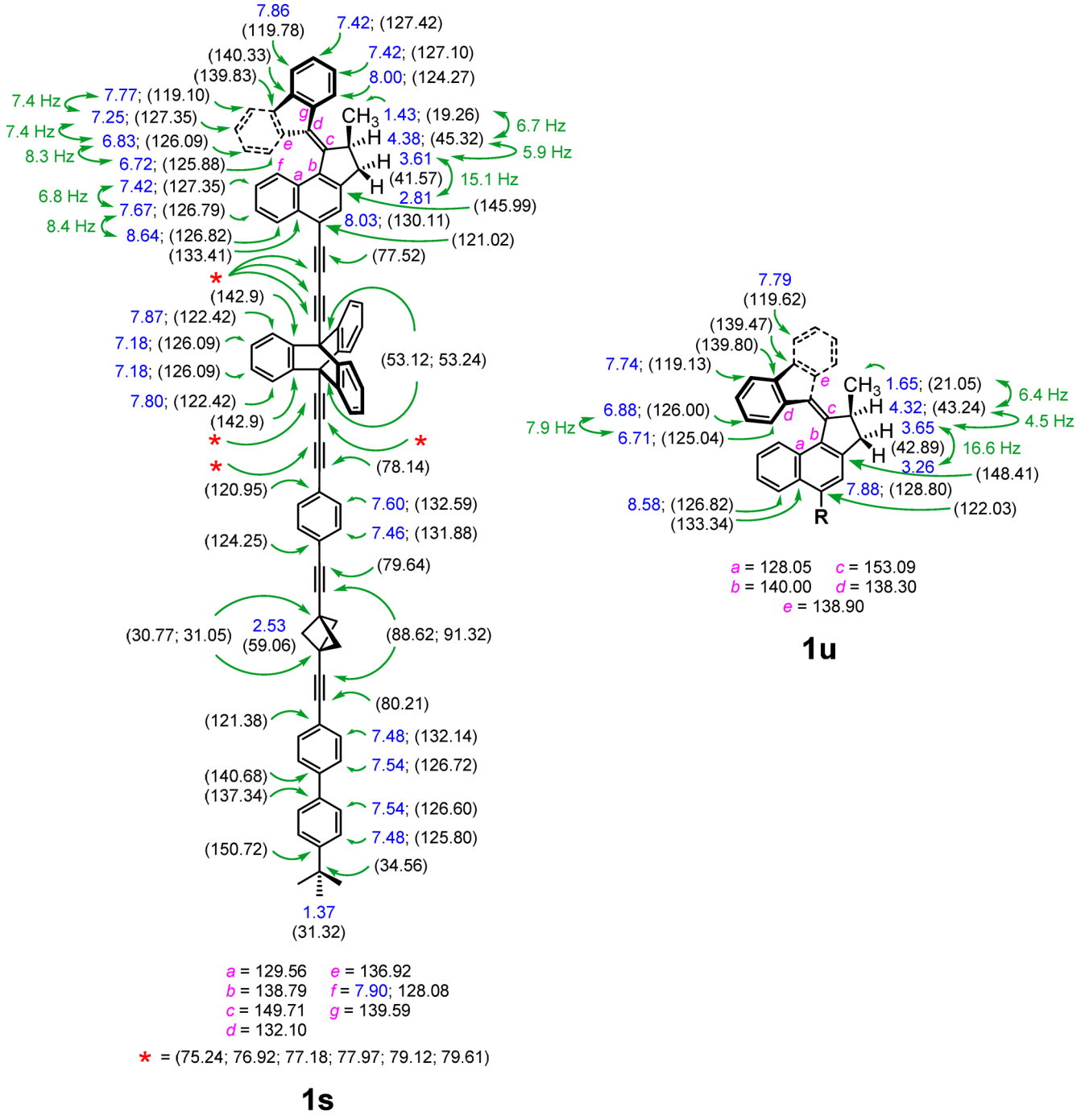

Figure 2. ^{1}H (blue) and ^{13}C (black) NMR assignment in **1s** ($CDCl_3$, 20 °C), and **1u** ($CDCl_3$, −20 °C). See the Supporting Information for the spectra.

bridgehead carbons are completely overlapped with the nearby peak of three equivalent methyl atoms of the *tert*-butyl group in ^{13}C CP MAS NMR of both neat **1s** and the two inclusion complexes. On the other hand, the signal of the three methylene bridges appears at 60.2 ppm in ^{13}C CP MAS NMR of neat **1s**, and is shifted upfield to 59.1 ppm in both 5%**1s**@TPP-d_{12}, and 10%**1s**@TPP-d_{12}.

The last characteristic feature originating in the nonpolar shaft are two resonances of triple bond carbons located next to the BCP cage. They give two signals at 88.6 and 91.3 ppm in $CDCl_3$ solution (purple peaks in Figure 3), but collapse to one peak at 90.9 ppm in ^{13}C CP MAS NMR of neat **1s**. They are absent in the spectra of 5%**1s**@TPP-d_{12}, and 10%**1s**@TPP-d_{12}.

In solution ^{13}C NMR spectra the triptycene unit produces two closely spaced aliphatic peaks at 53.1 and 53.2 ppm, due to the two chemically inequivalent bridgehead atoms. They collapse to one sharp peak at 52.6 ppm in solid-state NMR spectrum of neat **1s**, which is shifted downfield to 53.6 ppm in ^{13}C CP MAS NMR of 5%**1s**@TPP-d_{12}, and 10%**1s**@TPP-d_{12}.

The molecular motor part (d and e, Chart 1) is represented in the aliphatic region (Figure 2) by two resonances of carbon atoms of the indene unit (Figure 3, black signals of CH_2 at 41.6 ppm and CH at 45.3 ppm in $CDCl_3$ solution, and 41.2 and 44.7

DOI: 10.1021/jacs.7b05404
J. Am. Chem. Soc. 2017, 139, 10486−10498

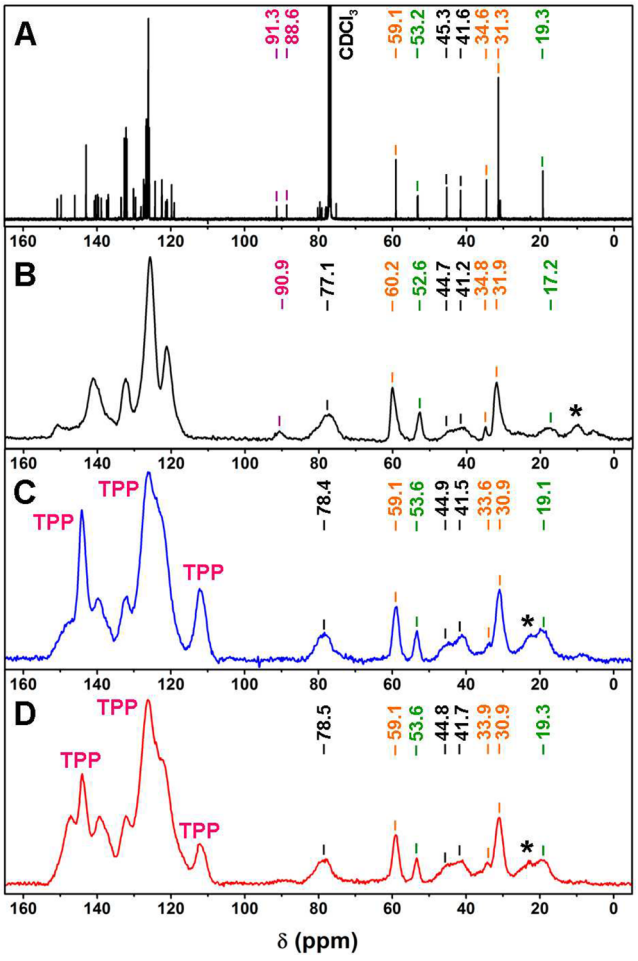

Figure 3. ^{13}C NMR spectra of **1s** in $CDCl_3$ solution (A), ^{13}C CP MAS NMR of neat **1s** (B), 5%**1s**@TPP-d_{12} (C), and 10%**1s**@TPP-d_{12} (D). The peaks marked by asterisks in panels B, C, and D are spinning sidebands of the most intense aromatic peak at ∼128 ppm.

ppm in solid-state NMR of neat sample), and one carbon atom of the methyl group (Figure 3, green signal at 19.3 ppm in solution and 17.2 ppm in the solid state). These three signals are much broader in all solid-state spectra compared to all previously discussed aliphatic peaks. The position of both indene peaks is almost identical in the neat sample and both inclusion complexes (5% and 10%**1s**@TPP-d_{12}), and ranges from 41.2 to 41.7 ppm in the first case, and from 44.7 to 44.9 ppm in the second case. The peak of the methyl group located at 19.3 ppm in solution is shifted significantly upfield to 17.2 ppm in the solid state NMR of neat **1s**, but moves back to higher chemical shift values in both inclusions (19.1 ppm in 5%**1s**@TPP-d_{12} and 19.3 ppm in 10%**1s**@TPP-d_{12}) (Figure 3).

All triple bond carbon signals are well resolved in solution NMR (Figure 2), and are located mostly near 77 ppm (Figure 3). They form one broad peak with a maximum at 77.1 ppm (black peak in Figure 3) in solid-state NMR of neat **1s** and are shifted downfield in ^{13}C CP MAS NMR of 5%**1s**@TPP-d_{12} (78.4 ppm), and 10%**1s**@TPP-d_{12} (78.5 ppm).

The three peaks marked by asterisks in Figure 3 (panels B, C, and D) are spinning sidebands of the most intense aromatic peak at ∼128 ppm. The corresponding mirror spinning sidebands are present at ∼240 ppm for the neat sample and at ∼230 ppm for both inclusion compounds (this region is not shown in Figure 3). The ^{13}C CP MAS NMR of **1s** was acquired with a spinning frequency of 14.5 kHz, and those of 5%**1s**@TPP-d_{12} and 10%**1s**@TPP-d_{12}, were measured at 13 kHz.

The ^{31}P SPE NMR spectrum of 5%**1s**@TPP-d_{12} (Figure 4A) shows one peak at 33.1 ppm characteristic of the three

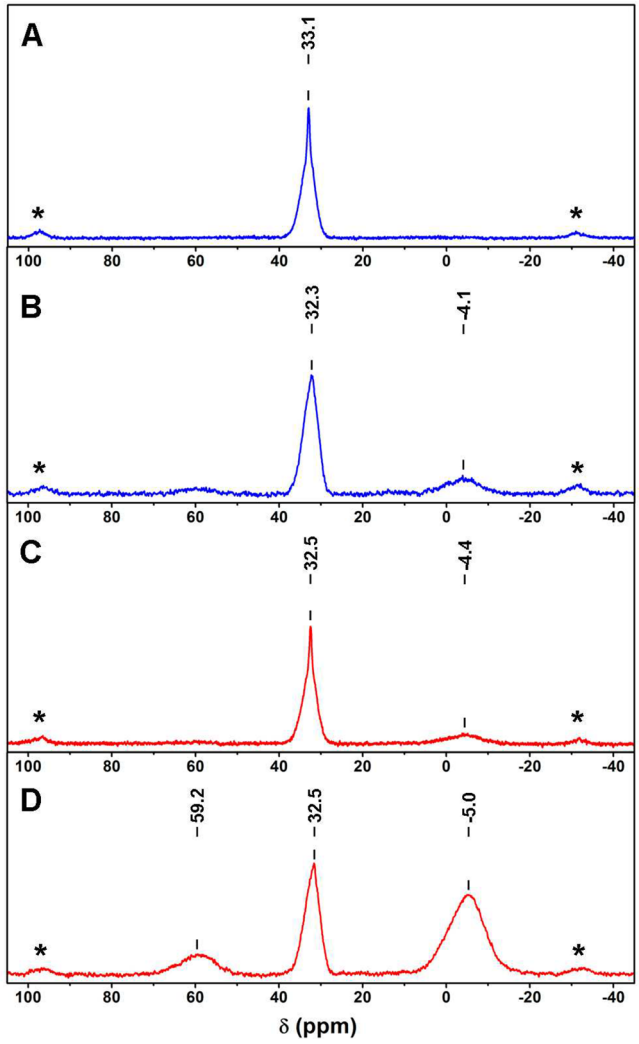

Figure 4. 5%**1s**@TPP-d_{12}: ^{31}P SPE NMR (A) and ^{31}P CP MAS NMR (B). 10%**1s**@TPP-d_{12}: ^{31}P SPE NMR (C) and ^{31}P CP MAS NMR (D). The peaks marked by asterisks are spinning sidebands.

crystallographically equivalent phosphorus nuclei in TPP. A similar spectrum was also obtained for 10%**1s**@TPP-d_{12}, but in this case a weak broad peak at −4.4 ppm is also observed (Figure 4C). The ^{31}P CP MAS NMR spectra of both 5%**1s**@TPP-d_{12} and 10%**1s**@TPP-d_{12} (Figure 4B,D) again contain a peak of phosphorus atoms present in hexagonal TPP at ∼32.4 ppm, and also an additional broad peak at −4.1 ppm for 5%**1s**@TPP-d_{12} (Figure 4B), and +59.2 and −5.0 ppm for 10%**1s**@TPP-d_{12} (Figure 4D). Their intensities are much lower in ^{31}P SPE measurements suggesting that hydrogen enriched impurities are present, most probably partially hydrolyzed TPP.

The presence of PO and POH bonds in 10%**1s**@TPP-d_{12} was confirmed by infrared spectroscopy in KBr pellet, which showed weak but characteristic stretching vibrations of ν(POH) at 3000−2500 cm^{-1}, and deformation vibrations of δ(PO) at 1006, 1000, and 930 cm^{-1}.

Transmission Electron Microscopy (TEM). was used to examine morphology of one of the inclusions (5%**1s**@TPP-

DOI: 10.1021/jacs.7b05404
J. Am. Chem. Soc. 2017, 139, 10486−10498

d_{12}). The sample consists of conglomerates of flat mostly circular discs with a 20−40 nm diameter and 10−20 nm thickness (Figure 5).

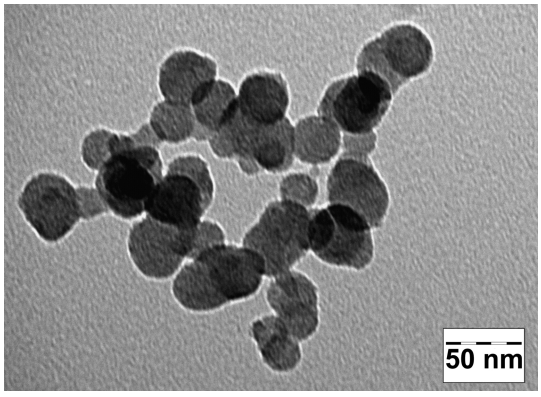

Figure 5. TEM of 5%**1**@TPP-d_{12}.

Differential Scanning Calorimetry (DSC). The DSC analysis of **1s** (Figure 6A) shows one small and broad exotherm

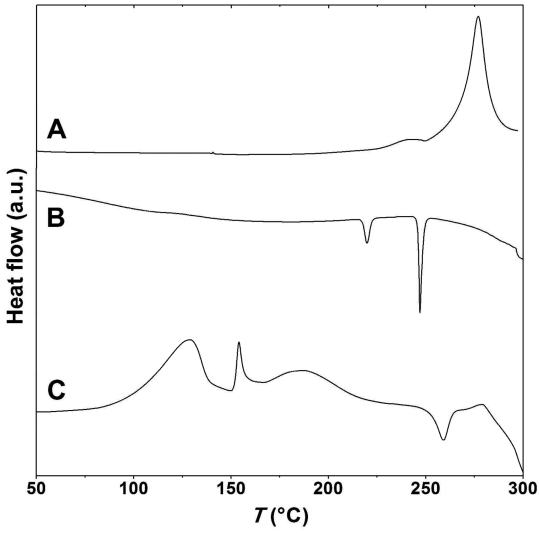

Figure 6. Differential scanning calorimetry traces from 50 to 300 °C: (A) neat **1s**, (B) guest-free TPP-d_{12}, and (C) 5%**1s**@TPP-d_{12}. Exotherms are positive peaks.

centered at ∼241 °C, and one strong exotherm at 277 °C, which could be attributed to explosive decomposition of the diethynyl substituted BCP cage. The peaks observed for neat TPP-d_{12} (Figure 6B) agree with previously published data,[59] and are interpreted as follows: a broad exotherm centered at ∼130 °C is associated with first-order transition of hexagonal TPP-d_{12} into its more stable monoclinic form. The endotherm at 220 °C corresponds to transition of monoclinic TPP-d_{12} back into its hexagonal form. The intense endotherm at 247 °C is due to melting. The DSC of 5%**1s**@TPP-d_{12} (Figure 6C, for full cyclic analysis see Figure S1 in Supporting Information) is more complex and consists of four exotherms (three broad peaks at 129, 187, and 279 °C, and a sharp one at 154 °C), and one endotherm at 259 °C, attributed to a melting of the inclusion. The exotherm at 129 °C probably corresponds to slow evaporation of water trapped inside the matrix and the hump at 279 °C is probably due to a decomposition of **1s**.

Powder X-ray Diffraction. In Figure 7 are shown the results of Cu Kα X-ray powder diffraction measurements of

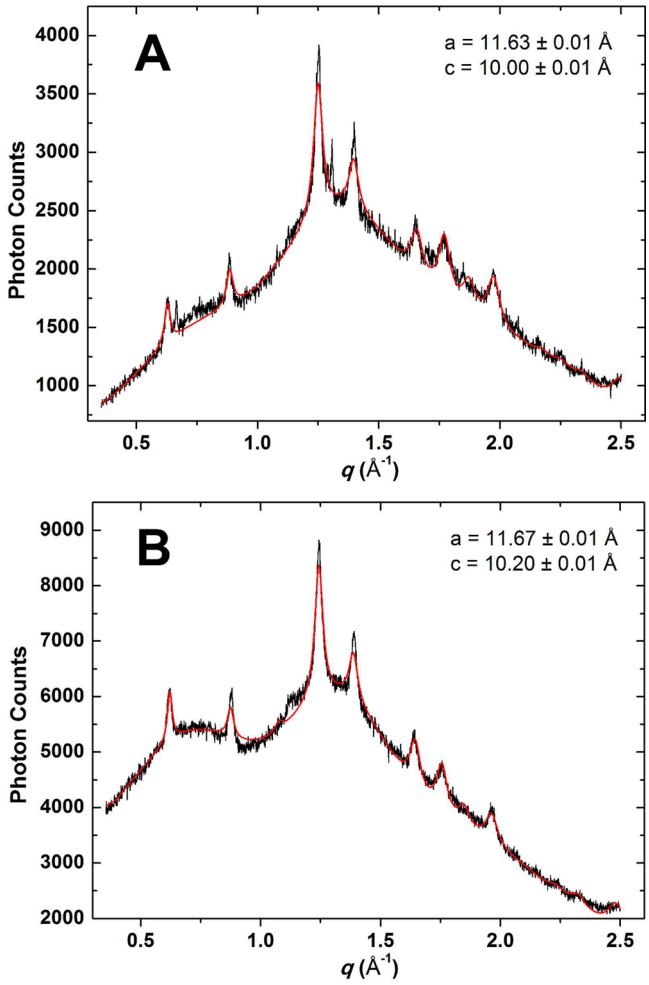

Figure 7. X-ray powder pattern for 5%**1s**@TPP-d_{12} (A) and 10%**1s**@TPP-d_{12} (B). The solid black line shows diffraction data. Red line is a fitting result assuming hexagonal peak positions and a measured background.

5%**1s**@TPP-d_{12} and 10%**1s**@TPP-d_{12}. The powder samples were those used to obtain the solid-state NMR spectra described above. The figure plots scattered X-ray photon counts against the magnitude of the scattering wave vector, q, in Å^{-1}. The latter is related to the scattering angle θ and to X-ray wavelength λ by $q = 4\pi \sin \theta/\lambda$. The inclusion compound 5%**1s**@TPP-d_{12} yielded a sequence of diffraction peaks (black solid line in Figure 7A) that are well explained by a simple hexagonal structure, and a broad background (fitting function is the red solid line), with lattice parameters that are expanded in the in-plane direction to 11.63 ± 0.01 Å, and slightly contracted in layer spacing of 10.00 ± 0.01 Å, respectively. This represents a 1% expansion and 1% contraction compared to the 11.496(1) Å and 10.129(1) Å reported for empty hexagonal TPP.[55] Two small and narrow peaks are observed for 5%**1s**@TPP-d_{12} at q values of 0.667 and 1.307 Å^{-1}, consistent with strong reflections from the monoclinic phase of TPP.[60] Figure 7B shows the scattering observed from 10%**1s**@TPP-d_{12}. Again, a set of diffraction peaks are observed that are well explained by a hexagonal material, but with slightly different lattice parameters of 11.67 ± 0.01 Å and 10.20 ± 0.01 Å for in-plane lattice

DOI: 10.1021/jacs.7b05404
J. Am. Chem. Soc. 2017, 139, 10486−10498

constant and hexagonal layer spacing, respectively. No monoclinic TPP peaks are observed for the 10%**1s**@TPP-d_{12} inclusion.

Rotation of 1 in Solution. *1. ^1H NMR.* Although all signals of hydrogen atoms present in the motor section of **1s** were assigned (Figure 2), only seven of them were used to demonstrate rotary motion of the fluorene rotor moiety (e, Chart 1) through their characteristic chemical shift changes (Figure 8A). Blue marked hydrogen atoms H_a–H_e and the CH_3 group are present on the indene stator part, whereas the hydrogen atom H_f is located on the fluorene rotor moiety (Figure 8). Irradiation of the sample (λ_{max} = 405 ± 5 nm) gave rise to an additional set of peaks marked as red H_a–H_f and CH_3 (Figure 8B), characteristic of **1u**. Reversion of **1u** back to **1s** in the dark was complete in $CDCl_3$ after 24 h at −10 °C (Figure 8C). The ratio **1s**/**1u** at the photostationary state was then determined by the integration of hydrogen signals characteristic for both rotor and stator parts (Chart 1) as depicted in Figure 8B.

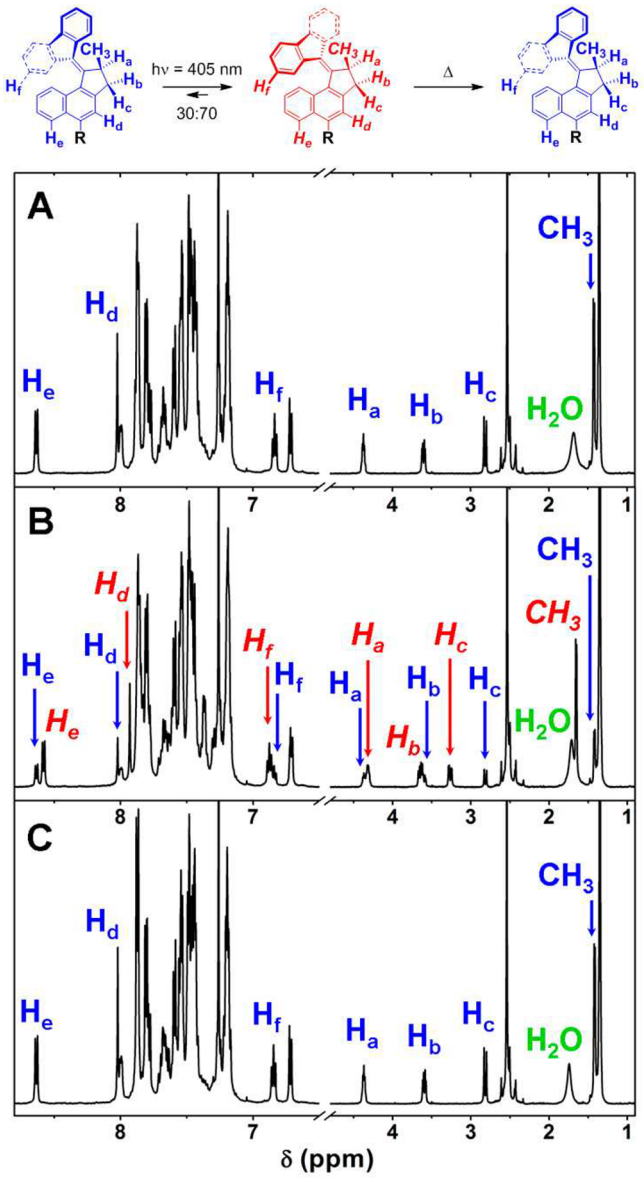

Figure 8. ^1H NMR spectra of **1** in $CDCl_3$ at −10 °C before irradiation (A), at the photostationary state (B), and after thermal relaxation (C). A single enantiomer is depicted.

2. UV–vis Spectroscopy. The thermal part of the rotation of the motor section in **1** (parts d and e, Chart 1) was also followed by UV–vis absorption spectroscopy. The UV–vis spectrum of **1s** in CH_2Cl_2 at 10 °C (Figure 9A) shows four absorption peaks with maxima at 280, 300, 318, and 425 nm (red line). Upon irradiation (λ_{max} = 405 ± 5 nm) and reaching the photostationary state (Figure 9A, blue line), two absorption peaks remained unchanged (300 and 318 nm), and two were red-shifted, one from 280 to 284 nm and the other from 425 to 440 nm. The presence of an isosbestic point at 448 nm (Figure 9B) indicates that the photochemical isomerization is a clean process. The bathochromic shift can be attributed to the formation of an unstable isomer **1u** with an enhanced twist of the central double bond.[61,62] The spectrum of **1u** (red) changed back to that of **1s** (blue) after the sample was left in the dark at 10 °C for 60 min (Figure 9B).

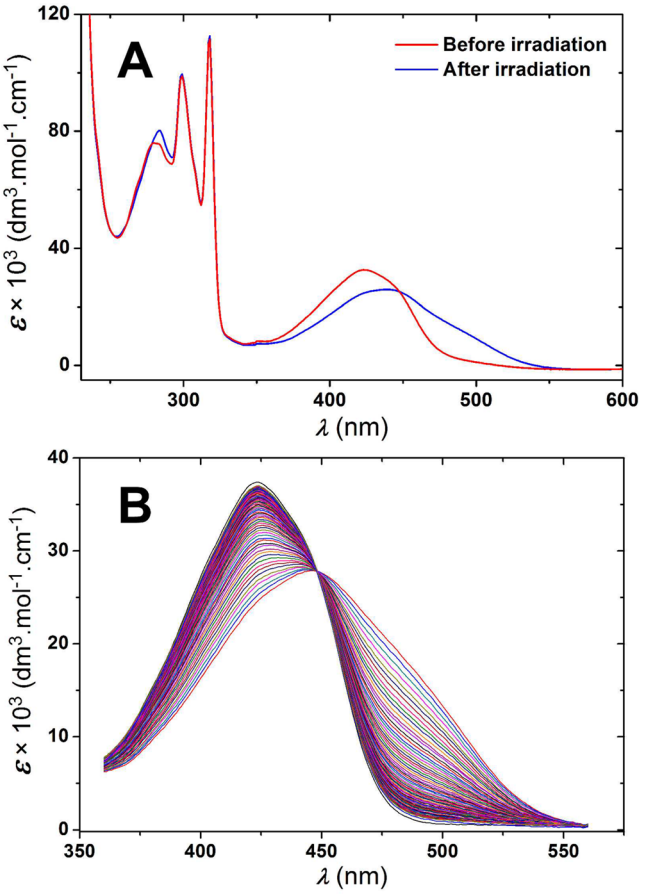

Figure 9. UV–vis absorption spectra of **1**. (A) Solution in CH_2Cl_2 at 10 °C before (red) and after (blue) irradiation. (B) Progress of thermal interconversion of **1u** to **1s** in CH_2Cl_2 at 10 °C.

UV–vis Analysis of Aqueous Suspensions of Inclusion Compound. The UV–vis spectra of both 5%**1s**@TPP-d_{12} and 10%**1s**@TPP-d_{12} suspended in water are identical and share characteristic features with **1s** in CH_2Cl_2 solution but are noisier, mostly due to lower concentration of the chromophore and to scattering. The UV–vis spectrum of 5%**1s**@TPP-d_{12} consists of three absorption bands with maxima at 302, 320, and 444 nm (Figure 10A, red). The absorption of TPP-d_{12} starts at 290 nm and thus overlaps with the peak at 284 nm,

DOI: 10.1021/jacs.7b05404
J. Am. Chem. Soc. 2017, 139, 10486–10498

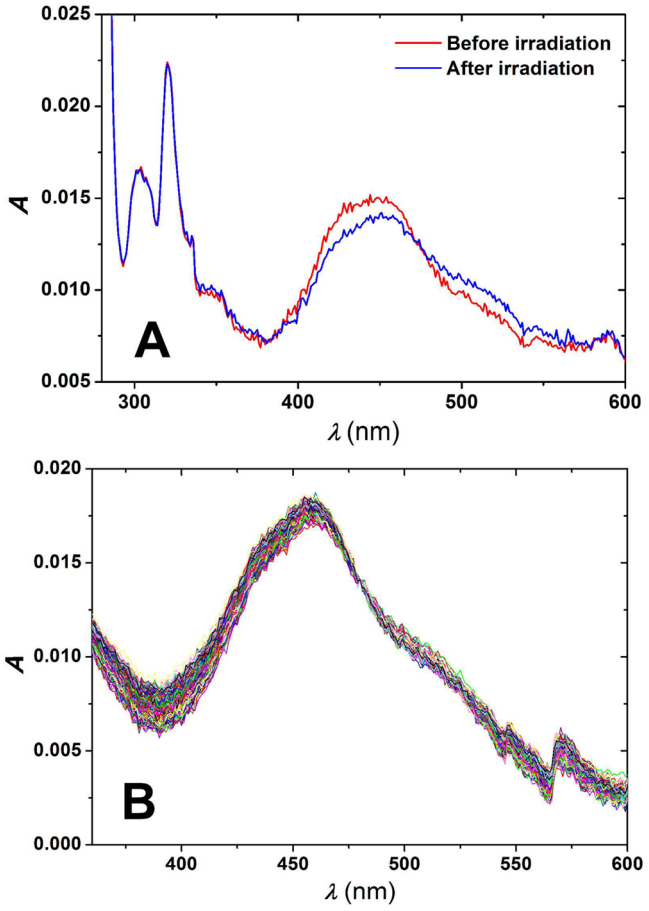

Figure 10. UV−vis absorption spectra of 5%**1**@TPP-d_{12}. (A) Suspension in water at 10 °C before (red) and after (blue) irradiation. (B) Progress of thermal interconversion of 5%**1u**@TPP-d_{12} to 5%**1s**@TPP-d_{12} in water at 10 °C.

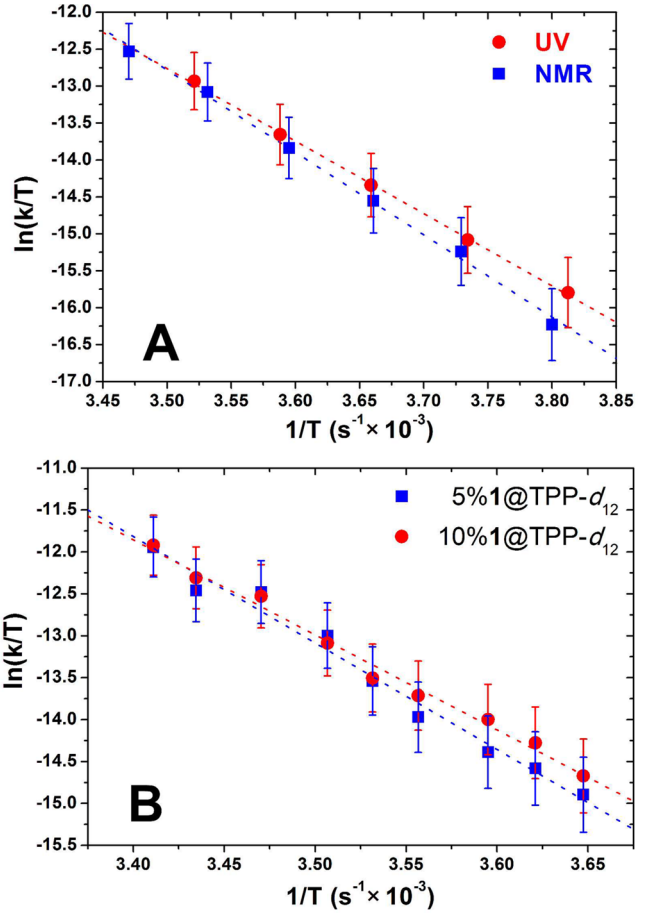

Figure 11. Eyring plots for the thermal helix inversion of **1u** to **1s**. (A) Solution of **1** in CH_2Cl_2 (red, UV−vis), and in $CDCl_3$ (blue, ^{1}H NMR). (B) UV−vis spectrum of a suspension of 5%**1**@TPP-d_{12} (blue), and 10%**1**@TPP-d_{12} (red).

which was characteristic for both **1s** and **1u** in CH_2Cl_2 solution. Irradiation of this sample (λ_{max} = 405 ± 5 nm) at 10 °C resulted in 5%**1u**@TPP-d_{12} (Figure 10A, blue) with two absorption maxima at 302 and 320 nm, which are unchanged from 5%**1s**@TPP-d_{12}, and one maximum that is red-shifted to 450 nm. Figure 10B shows representative time-dependent UV−vis spectra for the thermal transformation of 5%**1u**@TPP-d_{12} to 5%**1s**@TPP-d_{12} acquired at 10 °C, with an isosbestic point at 470 nm.

Since the photoisomerization step of the molecular motor occurs on a picosecond time scale,[63,64] the rate of the subsequent thermal helix inversion is rate limiting and determines the overall speed of rotation.[65,66] The kinetics of the slow step was studied by time-dependent ^{1}H NMR and UV−vis absorption spectroscopy in $CDCl_3$ or CH_2Cl_2 solution of **1** at several temperatures (in 5 °C intervals starting from −10 to +10 °C for ^{1}H NMR and from −10 to +15 °C for UV−vis). Kinetics of rotary motion of surface mounted molecular motors in 5%**1**@TPP-d_{12} and 10%**1**@TPP-d_{12} was studied only by UV−vis spectroscopy (at 1, 3, 5, 8, 10, 12, 15, 18, and 20 °C). These data yielded the half-life ($t_{1/2}$) and rate constant (k^0) at 20 °C and activation free energy ($\Delta G^{\ddagger}$), and enthalpy ($\Delta H^{\ddagger}$), for both motor in solution (Figure 11A) and included in a surface (Figure 11B, Table 1).

DISCUSSION

Synthesis. The present synthesis of **1s** confirms the generality of the previously developed modular approach[49] based on preparation of two reasonably soluble molecular fragments (bicyclo[1.1.1]pentane-based shaft **3** and triptycene stopper coupled with molecular motor **2**), whose Sonogashira cross-coupling performed at very mild conditions afforded the expected final product in excellent yield. The synthetic route to iodine-funtionalized second generation motor **4**, with the diazo−thioketone coupling as the key olefination step, provides ready access to a versatile motor for connecting to the triptycene stopper. The product is thus accessible on the scale of hundreds of milligrams.

Inclusion Compounds. The powder XRD revealed that both inclusion compounds contain almost exclusively the hexagonal form of TPP, with lattice parameters slightly expanded relative to guest-free material. This implies that the guest molecules are inserted into TPP channels and expand them.

The powder XRD results strongly support the identification of both 5%**1s**@TPP-d_{12} and 10%**1s**@TPP-d_{12} as surface inclusion compounds, where **1s** is localized at the surface of hexagonal TPP crystallites. The monoclinic structure of TPP is preferred over empty hexagonal TPP at temperatures below roughly 180 °C.[60] Molecules included into the hexagonal channels stabilize the hexagonal phase down to cryogenic

DOI: 10.1021/jacs.7b05404
J. Am. Chem. Soc. 2017, 139, 10486−10498

Table 1. Kinetic Results for Neat 1, 5% and 10%1@TPP-d_{12}[a]

	neat **1** in solution		5%**1**@TPP-d_{12}	10%**1**@TPP-d_{12}
	UV−vis (CH_2Cl_2)	^{1}H NMR ($CDCl_3$)	UV−vis (suspension in H_2O)	UV−vis (suspension in H_2O)
$\Delta G^{\ddagger}$ (kJ/mol)	87 ± 4	87 ± 6	87 ± 12	87 ± 6
$\Delta H^{\ddagger}$ (kJ/mol)	94 ± 2	82 ± 4	106 ± 6	94 ± 3
$t_{1/2}$ (20 °C, s)	303 ± 30	345 ± 20	369 ± 130	378 ± 65
k^0 (20 °C, s^{-1})	0.0023 ± 0.0002	0.0020 ± 0.0001	0.0019 ± 0.0006	0.0018 ± 0.0003

[a]For parent molecular motor (d and e in Chart 1), the following values were obtained: $\Delta G^{\ddagger}$ = 85 kJ/mol, k^0 = 0.0036 s^{-1}, and $t_{1/2}$ = 190 s.[67]

temperatures. The first diffraction peak, located at q values of ∼0.63 $Å^{-1}$, provides a confirmation of inclusion: in empty hexagonal TPP, this diffraction peak is particularly strong as it measures the modulation of electron density between the TPP walls and the essentially zero electron density in the empty channels. The modest height of this peak in the inclusion samples shows that the electron density in the channels is substantial, consistent with an inclusion compound. Finally, the broad diffraction peaks and rapid drop in peak intensity with increasing q values are consistent with an inclusion compound with a combination of significant strain and finite grain size and are in line with our experience with other surface inclusions in TPP,[47,49] as opposed to bulk inclusions.[54,68]

The TEM analysis showed that the texture of 5%**1s**@TPP-d_{12} is identical with those of previously prepared samples[54,68] and consists of discs of 20−40 nm diameter and approximately 10 nm thickness. The thickness was used to estimate maximum guest loading (Supporting Information). This value is roughly 10 mol % for 10 nm thick discs. The disc diameter then dictates the maximum available size for molecular motor arrays, which is ∼300−∼1300 nm^2 for circular particles with diameter 20−40 nm. Taking into account the surface occupied by a single channel, approximately 1.13 nm^2, one ideally flat and defect-free facet of a TPP disc can accommodate 300−1100 guest molecules on each side.

Based on previous experience, the observed relatively small size of TPP particles is typical of surface inclusions. The surface-mounted guest molecules locally expand lattice parameters in a few upper TPP layers and thus introduce surface strain, which fragments larger crystals.

Solid-State NMR. The measurements discussed so far provided information on the constitution, morphology, and type of inclusion of the samples, but not about the position of guest molecules within the TPP channels. Such information is provided by solid-state ^{13}C and ^{31}P NMR spectroscopy.

The ^{31}P SPE NMR spectra of both 5%**1s**@TPP-d_{12} and 10%**1s**@TPP-d_{12} confirmed the XRD result that both samples consist almost exclusively of hexagonal TPP. In NMR spectra this crystal form is characterized by a singlet at ∼33.0 ppm due to the three crystallographically equivalent phosphorus nuclei (Figure 4A,C). The spectrum of 10%**1**@TPP-d_{12} also contained an additional small and broad peak at −4.4 ppm, which results from slow hydrolysis, detected also by characteristic IR peaks. Signal intensity of phosphorus nuclei directly attached to OH groups was then enhanced in the ^{31}P CP MAS NMR spectrum (Figure 4D).

The ^{31}P CP MAS NMR spectra (Figure 4B,D) of both inclusion compounds contain a singlet at ∼32.4 ppm, which is also attributed to hexagonal TPP. The presence of this peak proves that the TPP channels contain hydrogen atoms carrying guest molecules that mediate through-space transfer of magnetization in the cross-polarization (CP) experiment.

Since the ^{13}C CP MAS NMR spectra of 5%**1s**@TPP-d_{12} and 10%**1s**@TPP-d_{12} are nearly identical and differ slightly only in intensities of TPP signals (Figure 3), the second sample will be used as representative in the discussion. Three peaks in the ^{13}C CP MAS NMR spectrum of neat **1s** that are due to characteristic groups in the nonpolar shaft (orange signals in Figure 3) are easily identified. They belong to the three equivalent methylene bridges of BCP at 60.2 ppm, the quaternary carbon atom of *tert*-butyl at 34.8 ppm, and the three equivalent methyl carbon atoms of *tert*-butyl at 31.9 ppm. All three are shifted upfield in 10%**1s**@TPP-d_{12} (59.1 ppm for BCP, and 33.9 and 30.9 ppm for *tert*-butyl unit). This result shows that this part of the guest molecule is inserted inside a TPP channel and is shielded by its aromatic rings. Similar trends are also visible in comparison of inclusion compound with **1s** in $CDCl_3$ solution where quaternary carbon of *tert*-butyl group is located at 34.6 ppm, three equivalent methyl groups at 31.3 ppm and three equivalent methylene groups of BCP at 59.1 ppm. In this case, both carbon resonances attributed from *tert*-butyl group are still upfield shifted and only the signal of BCP remains unchanged.

The observation that methylene carbon atoms in the BCP unit only gave one relatively sharp peak in the inclusion indicates that all BCP cages have the same chemical environment, and this most likely means that they are immersed into TPP channels to the same depth.

Both triple bond carbon atoms located next to BCP cage gave rise to one single peak at 90.9 ppm in the ^{13}C CP MAS NMR spectrum of neat **1s** (purple peak, Figure 3), but they are not visible in the spectrum of the inclusion compound. It is another indication that this part of the guest molecule has a different chemical environment in the inclusion compound than in the neat **1s** and confirms the conclusion that it is inserted inside the TPP-d_{12} channel. The nearest hydrogen atoms are located on the methylene groups of the BCP cage (ca. 3.2 Å distant), which can freely rotate, and thus prevent an effective transfer of magnetization via dipolar interaction under the contact time applied.

The two green peaks in Figure 3 belong to carbon atoms within the triptycene and motor units and are thus expected to be above the TPP surface. The peak of the triptycene bridgehead carbon atom is shifted from 53.6 ppm in inclusion to 52.6 ppm in the neat sample and also to 53.2 ppm relative to **1s** in solution. The signal of the fluorene methyl carbon changed from 19.3 ppm in inclusion to 17.2 ppm in neat **1s**, and remained unchanged compared to **1s** in $CDCl_3$ solution (19.3 ppm).

The presence of three relatively intense peaks of TPP-d_{12} in the ^{13}C CP MAS NMR spectra of both 5%**1s**@TPP-d_{12} and 10%**1s**@TPP-d_{12} (Figure 3C,D) represents an additional indirect proof that a surface inclusion is formed (the guest hydrogen atoms can be polarized and the polarization is then

DOI: 10.1021/jacs.7b05404
J. Am. Chem. Soc. 2017, 139, 10486−10498

transferred to carbon atoms of the host during the CP experiment).

Analysis of Thermal Helix Inversion. One 360° rotation cycle of the molecular motor consists of two steps. The first one, photochemical isomerization of **1s** to **1u**, occurs on a picosecond time scale,[63,64] whereas the second one, thermal helix inversion of **1u** back to **1s**, is much slower and can be easily monitored by ^{1}H NMR or UV−vis absorption spectroscopy.[57]

The ^{1}H NMR of **1** in $CDCl_3$ solution revealed that the ratio **1s**/**1u** at the photostationary state is about 30:70 (by integration of CH signals shown in Figure 8). The structure seems to be very stable and no traces of decomposition were detected even after more than 20 rotation cycles initiated by irradiation at 405 ± 5 nm at room temperature.

Eyring kinetic parameters characterizing the thermal part of rotary motion of **1** in solution were independently obtained by ^{1}H NMR and UV−vis absorption spectroscopy (Table 1). The two methods provided comparable results, similar to those of the parent motor (d and e sections of Chart 1).[57,67] This observation is not surprising because the geometry of the molecule does not allow mechanical interference between the rotor and the anchoring units (a, b, and c in Chart 1) attached to the stator part (d in Chart 1).

In CH_2Cl_2 solution, **1u** is characterized by absorption at 440 nm, and the disappearance of this peak signifies the end of the rotation cycle and renewed formation of **1s** with its characteristic absorption at 425 nm. An identical spectral behavior was observed also for aqueous suspensions of both inclusion compounds, 5%**1**@TPP-d_{12} and 10%**1**@TPP-d_{12}. The only difference was that their absorption maxima were red-shifted for **1s** from 425 to 444 nm and for **1u** from 440 to ∼450 nm. This is likely due to excitonic interactions between the closely packed chromophores. The kinetic parameters are nearly identical for both inclusion compounds and for **1** in solution (Table 1), demonstrating that the anchoring to the surface and the degree of surface saturation do not affect the functionality of these surface-mounted molecular devices.

SUMMARY

We have designed and synthesized a unidirectional light-driven molecular motor suitable for host−guest surface inclusion complexes with tris(*o*-phenylene)cyclotriphosphazene (TPP). The motor molecules form two-dimensional trigonal arrays covering the large facets of disc-shaped TPP crystals. The kinetics of the thermal step in the rotation of motors is independent of the degree of coverage (50 vs 100%) and is similar to that observed in solution. The system presented here provides a versatile way to 2D surface confinement with precise ordering of rotary molecular motors.

EXPERIMENTAL SECTION

Materials. All reactions were carried out under argon atmosphere with dry solvents freshly distilled under anhydrous conditions, unless otherwise noted. Standard Schlenk and vacuum line techniques were employed for all manipulations of air- or moisture-sensitive compounds. Yields refer to isolated, chromatographically, and spectroscopically homogeneous materials.

1-((4′-*tert*-Butylbiphenyl-4-yl)ethynyl)-3-((4-iodophenyl)ethynyl)-bicyclo[1.1.1]pentane (**3**),[49,69] 5-bromo-2-methyl-2,3-dihydrocyclopenta[*a*]naphthalen-1-one (**6**),[57] 9-diazo-9*H*-fluorene (**8**),[57] and 9-((trimethylsilyl)buta-1,3-diynyl)-10-(buta-1,3-diynyl)-triptycene (**10**)[49] were synthesized according to published procedures. TPP-d_{12} was synthesized from catechol-d_6 according to a published procedure.[47,49] The code for designating an inclusion compound is X %**1**@TPP-d_{12}, where X is the molar percentage of rotor **1s**.

THF and ether were dried over sodium with benzophenone and distilled under argon prior to use. Triethylamine was dried over CaH_2 and distilled under argon prior to use. Toluene and 1,4-dioxane were dried over sodium and distilled under argon prior to use. All other reagents were used as supplied.

Procedures. Analytical thin-layer chromatography (TLC) was performed using precoated TLC aluminum sheets (Silica gel 60 F_{254}). TLC spots were visualized using either UV light (254 nm) or a 5% solution of phosphomolybdic acid in ethanol and heat (200 °C) as a developing agent. Flash chromatography was performed using silica gel (high purity grade, pore size 60 Å, 70−230 mesh). Melting points are reported uncorrected. Infrared spectra (IR) were recorded in KBr pellets. Chemical shifts in ^{1}H, and ^{13}C NMR spectra are reported in ppm on the δ scale relative to $CHCl_3$ (δ = 7.26 ppm for ^{1}H NMR and δ = 77.0 ppm for ^{13}C NMR). Splitting patterns are assigned s = singlet, d = doublet, t = triplet, m = multiplet, br = broad signal.

High-resolution mass spectra (HRMS) using atmospheric-pressure chemical ionization (APCI) and electrospray ionization (ESI) were obtained on a mass analyzer combining linear ion trap and the Orbitrap, and those using electron ionization (EI) and chemical ionization (CI) mode were taken on a time-of-flight mass spectrometer.

The published procedure[47] for preparing the inclusion compounds from components was modified as follows. The neat rotor **1s** (11.57 mg for 5 mol % inclusion, and 23.14 mg for 10 mol % inclusion), and neat solvent-free hexagonal TPP-d_{12} (100 mg, 0.212 mmol) were mixed and ball-milled six times in 5 min intervals in a stainless steel ball mill. Between each of those periods, the sample was thoroughly scratched from the mill walls. The resulting fine orange powder was recovered and placed into a small vial wrapped in aluminum foil. The vial was inserted into a small flask and the vacuum/argon cycle was applied three times. The flask was then tightly closed, and annealed under argon for 24 h at 70 °C in an oven.

Solid-State NMR. High-resolution ^{13}C and ^{31}P solid-state NMR spectra were obtained using a Bruker Avance II spectrometer operating at 125.7 MHz for ^{13}C, 202.4 MHz for ^{31}P, and 499.9 MHz for ^{1}H. Samples were packed into 3.2 mm magic angle spinning (MAS) rotors and measurements taken at a MAS rate of 13−14.5 kHz using cross-polarization (CP) or direct excitation. The typical CP conditions used were: recycle delay 4 s, contact time 2 ms, acquisition time 30 ms. The ^{13}C spectra were referenced with respect to external neat tetramethylsilane by setting the carbonyl signal from a replacement sample of α-glycine to 176.03 ppm. Phosphorus spectra were referenced with $(NH_4)_2HPO_4$ (δ = 1.37 ppm). The assignment of the ^{13}C ss-NMR signals was based on comparison with solution-state spectrum and short CP MAS measurements (contact time 40 μs), where only signals of carbon atoms directly attached to a hydrogen are observable.

UV Analysis. Temperature-dependent UV−vis spectra were recorded using a Varian Cary 5000 spectrophotometer equipped with Cary WinUV software. Cooling and temperature stabilization were achieved with custom-made copper cell holder mounted on a water-cooled Peltier element. The cell holder contained three windows in a T-shaped arrangement. Two were used for absorption measurements and the third one, perpendicular to the previous two, for sample excitation.

The Peltier element was powered with a HCS 3200 power supply. A commercial thermometer TM-RS232 was used for temperature measurements with a precision of 0.1 °C. The thermometer and the power supply were connected to a PC via COM ports and controlled with custom written software for temperature stabilization. Standard temperature deviation was 0.06 °C over the whole measured region.

The sample was excited with a 1 W laser operating at 405 ± 5 nm. The photostationary state in both solution and suspension was reached in ∼7 s, and all samples were irradiated for 20 s before kinetic measurement. The measurements were taken in a cyclic mode, in predefined time intervals.

DOI: 10.1021/jacs.7b05404
J. Am. Chem. Soc. 2017, 139, 10486−10498

The same laser was also used for irradiation of the sample in NMR tube for the NMR determination of reaction kinetics. The irradiation time was 5 min and the sample was cooled to −40 °C during the irradiation.

Transmission Electron Microscopy. The samples were prepared by dropping an aqueous suspension of 5%**1s**@TPP-d_{12} onto a carbon-coated copper grid and drying in air. Images were recorded with a JEOL JEM-1011 transmission electron microscope operated at 60 kV.

DSC Analysis. was performed on a DSC Q20 (TA Instruments). Neat **1s** (4.4 mg), and TPP-d_{12} (5.8 mg) were heated separately from room temperature to 300 °C at 10 °C/min. Analysis of the surface inclusion 5%**1s**TPP-d_{12} (5.5 mg) consisted of three parts at 10 °C/min. The first part was heating from room temperature to 310 °C, the second was cooling to 40 °C, and the third was warming to 310 °C.

Powder X-ray Diffraction. The X-ray powder patterns were taken with Bruker D8 Discoverer powder diffractometer using Cu Kα radiation at a wavelength of λ = 0.154 18 nm and line detector LYNXEYE XE. Powder samples were loaded on silicon holder (6° off cut from (111)). The measurement was performed in the range of 5−80° 2θ with a step 0.02° 2θ and 1 s/step measurement time.

*Synthesis. Molecular Motor **1**.* A flame-dried Schlenk flask was charged with **3** (100 mg, 0.190 mmol, 1.0 equiv), **2** (150 mg, 0.217 mmol, 1.1 equiv), $Pd(PPh_3)_4$ (9 mg, 0.008 mmol, 4 mol %), and CuI (1 mg, 0.006 mmol, 3 mol %). After three successive vacuum/argon cycles, degassed dry THF (10 mL) and triethylamine (5 mL) were added from a syringe. The yellow solution was stirred for 16 h at room temperature. A dense white solid precipitated. Addition of methanol (20 mL) caused precipitation of orange solid. The crude reaction mixture was centrifugated to remove solvents (10 min, 5000 rpm). The orange solid residue was placed on a frit and washed with concentrated aqueous NH_4Cl (2 × 10 mL), water (2 × 15 mL), methanol (2 × 15 mL), acetone (2 × 10 mL), ether (2 × 5 mL), hexane (2 × 10 mL), and finally dried using Kugelrohr distillation apparatus (60 min, 80 °C, 500 mTorr). The molecular motor **1** was obtained as an orange crystalline solid (152 mg, 0.139 mmol, 73%).

Mp > 210 °C (dec.). ^{1}H NMR (500 MHz, $CDCl_3$): δ 1.37 (s, 9H), 1.44 (d, J = 6.7 Hz, 3H), 2.53 (s, 6H), 2.83 (d, J = 15.2 Hz, 1H), 3.61 (dd, J_1 = 5.4 Hz, J_2 = 15.0 Hz, 1H), 4.35−4.40 (m, 1H), 6.71−6.73 (m, 1H), 6.81−6.85 (m, 1H), 7.17−7.20 (m, 6H), 7.23−7.25 (m, 1H), 7.40−7.49 (m, 9H), 7.53−7.55 (m, 4H), 7.59−7.61 (m, 2H), 7.66−7.69 (m, 1H), 7.76−7.78 (m, 1H), 7.80−7.82 (m, 3H), 7.85−7.88 (m, 4H), 7.89−7.91 (m, 1H), 7.99−8.01 (m, 1H), 8.03 (s, 1H). ^{13}C NMR (125 MHz, $CDCl_3$): δ 19.3, 30.8, 31.1, 31.3, 34.6, 41.6, 45.3, 53.1, 53.2, 59.1, 75.2, 76.9, 77.5, 78.0, 78.1, 79.1, 79.61, 79.64, 80.2, 88.6, 91.3, 119.1, 119.8, 120.9, 121.0, 121.4, 122.41, 122.43, 124.2, 124.3, 125.8, 125.9, 126.1, 126.6, 126.7, 126.78, 126.81, 127.1, 127.3, 127.36, 127.41, 128.1, 129.6, 130.1, 131.9, 132.10, 132.13, 132.6, 133.4, 136.9, 137.3, 138.8, 139.6, 139.8, 140.3, 140.7, 142.92, 142.94, 146.0, 149.7, 150.7. IR (KBr): 3057, 2962, 2913, 2869, 2225, 2148, 1607, 1587, 1571, 1494, 1475, 1460, 1452, 1447, 1403, 1393, 1363, 1340, 1302, 1261, 1201, 1156, 1137, 1116, 1095, 1031, 1011, 1004, 946, 935, 921, 870, 854, 837, 821, 789, 777, 765, 750, 731, 710, 693, 674, 661, 647, 639, 621, 572, 543, 510, 494, 480 cm^{-1}. MS, m/z (%): 1091.5 (100, M + H). HRMS, (APCI) for ($C_{86}H_{58}$ + H^+): calcd 1091.46113, found 1091.46096. Anal. Calcd for $C_{86}H_{58}$: C, 94.64; H, 5.36. Found: C, 94.78; H, 5.44.

*9-((1-(9H-Fluoren-9-ylidene)2-methyl-2,3-dihydro-1Hcyclopenta-[a]naphthalen-5-yl)buta1,3-diyn-1-yl)10-(buta-1,3-diyn-1-yl)9,10-dihydro-9,10-[1,2]benzanthracene (**2**).* To a stirred solution of **11** (240 mg, 0.314 mmol, 1.0 equiv) in wet THF (5 mL) was added a solution of TBAF in THF (1.0 M, 376 μL, 0.376 mmol, 1.2 equiv) at room temperature. The brown reaction mixture was stirred for 30 min and was then diluted with CH_2Cl_2 (50 mL), washed with water (1 × 20 mL) and the organic phase was dried over $MgSO_4$. Solvents were removed under reduced pressure and column chromatography on silica gel (hexane/CH_2Cl_2, 3:1) afforded **2** as an orange crystalline solid (201 mg, 0.290 mmol, 92%).

Mp > 250 °C (dec.). ^{1}H NMR (500 MHz, $CDCl_3$): δ 1.44 (d, J = 6.75 Hz, 3H), 2.45 (s, 1H), 2.81 (d, J = 15.1 Hz, 1H), 3.62 (dd, J_1 = 5.6 Hz, J_2 = 15.1 Hz, 1H), 4.36−4.41 (m, 1H), 6.73−6.74 (m, 1H), 6.83−6.86 (m, 1H), 7.16−7.22 (m, 6H), 7.24−7.27 (m, 1H), 7.41−7.46 (m, 3H), 7.66−7.70 (m, 1H), 7.77−7.79 (m, 4H), 7.86−7.89 (m, 4H), 7.90−7.92 (m, 1H), 8.00−8.02 (m, 1H), 8.04 (s, 1H). ^{13}C NMR (125 MHz, $CDCl_3$): δ 19.2, 41.5, 45.3, 52.6, 53.2, 67.6, 68.6, 71.2, 76.5, 77.2, 77.5, 79.0, 79.6, 119.1, 119.8, 121.0, 122.3, 122.4, 124.3, 125.9, 126.08, 126.12, 126.8, 127.1, 127.3, 127.35, 127.41, 128.1, 129.5, 130.1, 132.1, 133.4, 136.9, 138.8, 139.6, 139.8, 140.3, 142.6, 142.9, 146.0, 149.7. IR (KBr): 3271, 3060, 3033, 3017, 2963, 2927, 2867, 2235, 2150, 1607, 1588, 1569, 1507, 1475, 1460, 1452, 1447, 1444, 1370, 1349, 1340, 1302, 1248, 1227, 1166, 1152, 1057, 1032, 986, 943, 905, 876, 861, 788, 778, 754, 751, 731, 710, 674, 647, 639, 621, 614, 566, 506, 496, 477 cm^{-1}. MS, m/z (%): 692.3 (100, M^+). HRMS, (MALDI) for ($C_{55}H_{32}^+$): calcd 692.2499, found 692.2510. Anal. Calcd for $C_{55}H_{32}$: C, 95.34; H, 4.66. Found: C, 95.51; H, 4.86.

*9-(5-Iodo-2-methyl-2,3-dihydrocyclopenta[a]naphthalen-1-ylidene)-9H-fluorene (**4**).* To a solution of **9** (60 mg, 0.142 mmol) in 1,4-dioxane (30 mL), NaI (212 mg, 1.414 mmol), CuI (27 mg, 0.142 mmol), and *trans-N,N′*-dimethylcyclohexane-1,2-diamine (100 μL, 0.634 mmol) were added. The mixture was stirred at 140 °C for 24 h in a sealed tube. After cooling to room temperature, the content was poured into water. After extraction with $CHCl_3$ (3 × 10 mL), the combined organic layers were washed with brine and dried over Na_2SO_4. The solvent was removed and the residue was purified by flash chromatography on silica gel (pentane/ethyl acetate, 90:1) to yield **4** as a dark red solid (60 mg, 0.128 mmol, 90%).

^{1}H NMR (500 MHz, $CDCl_3$): δ 1.39 (d, J = 6.7 Hz, 3H), 2.73 (d, J = 15.2 Hz, 1H), 3.56 (dd, J_1 = 5.7 Hz, J_2 = 15.1 Hz, 1H), 4.29−4.38 (m, 1H), 6.64 (d, J = 8.0 Hz, 1H), 6.78 (ddd, J_1 = 1.2 Hz, J_2 = 7.3 Hz, J_3 = 8.4 Hz, 1H), 7.20−7.24 (m, 1H), 7.34 (ddd, J_1 = 1.2 Hz, J_2 = 6.8 Hz, J_3 = 8.3 Hz, 1H), 7.38−7.43 (m, 2H), 7.54 (ddd, J_1 = 1.2 Hz, J_2 = 6.9 Hz, J_3 = 8.4 Hz, 1H), 7.71−7.79 (m, 2H), 7.79−7.87 (m, 1H), 7.91−8.02 (m, 1H), 8.21−8.23 (m, 2H). ^{13}C NMR (125 MHz, $CDCl_3$): δ 19.2, 41.4, 45.5, 102.5, 119.0, 119.7, 124.1, 125.7, 126.0, 127.0, 127.14, 127.17, 127.22, 127.4, 128.0, 130.2, 131.3, 132.8, 133.1, 135.7, 136.9, 137.7, 139.6, 139.7, 140.2, 147.8, 149.7. IR (KBr): 3049, 3013, 2962, 2924, 2849, 1617, 1608, 1578, 1561, 1515, 1456, 1438, 1402, 1370, 1341, 1302, 1274, 1211, 1146, 1060, 1009, 982, 941, 868, 814, 785, 773, 752, 735, 710, 686, 657, 643, 596 cm^{-1}. MS, m/z (%): 470.1 (100, M), 455.0 (47), 328.1 (68), 179.1 (10), 127.9 (12). HRMS, (EI) for ($C_{27}H_{19}I^+$): calcd 470.0532, found 470.0533.

*9-(5-Bromo-2-methyl-2,3-dihydrocyclopenta[a]naphthalen-1-ylidene)-9H-fluorene (**9**).* To a solution of ketone **6** (190 mg, 0.691 mmol) in toluene (10 mL) was added Lawesson's reagent (415 mg, 1.026 mmol). The mixture was stirred at reflux for 2 h and the solvent was evaporated. The residue was purified by column chromatography on silica gel (pentane/ethyl acetate, 30:1) to obtain a blue solution of thioketone **7**. The solvents were removed and a solution of 9-diazo-9*H*-fluorene (**8**) (263 mg, 1.368 mmol) in toluene (20 mL) was immediately added to the residue. The reaction mixture was heated at reflux overnight. The solvent was evaporated and the residue was purified by column chromatography on silica gel (pentane/ethyl acetate, 90:1) to yield **9** as a light yellow solid (60 mg, 0.142 mmol, 21%).

^{1}H NMR (400 MHz, $CDCl_3$): δ 1.40 (d, J = 6.7 Hz, 3H), 2.75 (d, J = 15.2 Hz, 1H), 3.59 (dd, J_1 = 5.7 Hz, J_2 = 15.2 Hz, 1H), 4.17−4.54 (m, 1H), 6.66 (d, J = 7.92 Hz, 1H), 6.80 (ddd, J_1 = 1.2 Hz, J_2 = 7.2 Hz, J_3 = 8.1 Hz, 1H); 7.24 (dd, J_1 = 5.1 Hz, J_2 = 12.6 Hz, 1H), 7.34−7.44 (m, 3H), 7.58 (ddd, J_1 = 1.1 Hz, J_2 = 7.1 Hz, J_3 = 8.3 Hz, 1H), 7.74−7.86 (m, 3H), 7.92 (s, 1H), 7.96−7.99 (m, 1H), 8.38 (d, J = 8.5 Hz, 1H). ^{13}C NMR (100 MHz, $CDCl_3$): δ 19.2, 41.7, 45.5, 119.0, 119.7, 124.1, 125.3, 125.7, 126.0, 126.7, 127.0, 127.1, 127.2, 127.4, 127.8, 127.9, 128.3, 130.7, 130.8, 131.1, 136.6, 137.0, 139.6, 139.7, 140.2, 147.3, 149.8. HRMS, (ESI) for ($C_{27}H_{19}Br$ + H^+): calcd 423.0748, found 423.0739.

*((10-((1-(9H-Fluoren-9-ylidene)2methyl2,3dihydro1Hcyclopenta-[a]naphthalen5-yl)buta1,3-diyn-1-yl)9,10-[1,2]benzanthracen-9-(10H)-yl)buta-1,3-diyn-1-yl)trimethylsilane (**11**).* A flame-dried Schlenk flask was charged with **4** (180 mg, 0.383 mmol, 1.0 equiv), 9-((trimethylsilyl)buta-1,3-diynyl)-10-(buta-1,3-diynyl)triptycene (**10**) (178 mg, 0.421 mmol, 1.1 equiv), $Pd(PPh_3)_4$ (18 mg, 0.015 mmol, 4

DOI: 10.1021/jacs.7b05404
J. Am. Chem. Soc. 2017, 139, 10486−10498

mol %), and CuI (2 mg, 0.011 mmol, 3 mol %). After three successive vacuum/argon cycles, dry and degassed THF (10 mL) and triethylamine (5 mL) were added from a syringe. The deeply orange solution was stirred for 18 h at room temperature. A dense white solid precipitated. The crude reaction mixture was diluted with CH_2Cl_2 (60 mL), washed with saturated aqueous NH_4Cl (2 × 30 mL), and dried over $MgSO_4$. Column chromatography on silica gel (hexane/CH_2Cl_2, 3:1) yielded **11** as an orange crystalline solid (249 mg, 0.325 mmol, 85%).

Mp > 250 °C (dec.). ^{1}H NMR (400 MHz, $CDCl_3$): δ 0.38 (s, 9H), 1.44 (d, J = 6.7 Hz, 3H), 2.82 (d, J = 15.1 Hz, 1H), 3.62 (dd, J_1 = 5.7 Hz, J_2 = 15.1 Hz, 1H), 4.35−4.42 (m, 1H), 6.73−6.75 (m, 1H), 6.83−6.87 (m, 1H), 7.15−7.22 (m, 6H), 7.24−7.28 (m, 1H), 7.41−7.47 (m, 3H), 7.67−7.70 (m, 1H), 7.78−7.81 (m, 4H), 7.87−7.89 (m, 4H), 7.91−7.93 (m, 1H), 8.01−8.03 (m, 1H), 8.04 (s, 1H). ^{13}C NMR (100 MHz, $CDCl_3$): δ −0.3, 19.2, 41.6, 45.3, 52.8, 53.2, 72.3, 77.2, 77.3, 77.5, 79.1, 79.6, 87.5, 87.7, 119.1, 119.8, 121.0, 122.38, 122.40, 124.3, 125.9, 126.1, 126.78, 126.81, 127.1, 127.3, 127.36, 127.41, 128.1, 129.6, 130.1, 132.1, 133.4, 136.9, 138.8, 139.6, 139.8, 140.3, 142.88, 142.90, 146.0, 149.7. IR (KBr): 3060, 3034, 3017, 2958, 2924, 2866, 2849, 2235, 2107, 1606, 1586, 1568, 1507, 1475, 1459, 1452, 1447, 1444, 1372, 1349, 1340, 1304, 1251, 1154, 1125, 1105, 1032, 1025, 945, 904, 845, 788, 778, 752, 731, 710, 697, 674, 639, 621, 614, 565, 479 cm^{-1}. MS, m/z (%): 764.3 (100, M^+). HRMS, (MALDI) for ($C_{58}H_{40}Si^+$): calcd 764.2894, found 764.2885. Anal. Calcd for $C_{58}H_{40}Si$: C, 91.06; H, 5.27. Found: C, 91.22; H, 5.37.

■ ASSOCIATED CONTENT

Supporting Information

The Supporting Information is available free of charge on the ACS Publications website at DOI: 10.1021/jacs.7b05404.

Copies of ^{1}H, ^{13}C NMR spectra of all new compounds (**1s**, **2**, **4**, **9**, and **11**), ^{1}H and ^{13}C NMR assignments in **1s**, **11**, and partial assignment in **1u** (PDF)

■ AUTHOR INFORMATION

Corresponding Authors

*kaleta@uochb.cas.cz

*b.l.feringa@rug.nl

ORCID

Jiří Kaleta: 0000-0002-5561-7580

Jiawen Chen: 0000-0002-0251-8976

Martin Dračínský: 0000-0002-4495-0070

Ben L. Feringa: 0000-0003-0588-8435

Josef Michl: 0000-0002-4707-8230

Notes

The authors declare no competing financial interest.

■ ACKNOWLEDGMENTS

This work was supported by the Institute of Organic Chemistry and Biochemistry, Academy of Sciences of the Czech Republic (RVO: 61388963). C. T. Rogers and J. Michl gratefully acknowledge financial support from the US National Science Foundation Division of Materials Research through Grants DMR-1409981 and DMR-1608424. B. L. Feringa and J. Chen gratefully acknowledge The Netherlands Organization for Scientific Research (NWO-CW), the European Research Council (ERC; advanced grant no. 694345 to B.L.F.) and the Ministry of Education, Culture and Science (Gravitation program no. 024.001.035). M. Dračínský gratefully acknowledges the Czech Science Foundation (grant no. 15-11223S). We are grateful to Dr. Lucie Bednárová for help with IR spectra, Dr. Radek Pohl for help with NMR spectra, Dr. Zdeněk Sofer for access to powder X-ray diffractometer, Dr. Paul I. Dron for preliminary solid-state NMR measurements, and Dr. Monika Benkovičová for acquiring TEM images.

■ REFERENCES

(1) Browne, W. R.; Feringa, B. L. *Nat. Nanotechnol.* **2006**, *1*, 25.

(2) *From Non-Covalent Assemblies to Molecular Machines*; Sauvage, J. P., Gaspard, P., Eds; Wiley-VCH: Weinheim, Germany, 2010.

(3) *Molecular Devices and Machines: Concepts and Perspectives for the Nanoworld*; Balzani, V., Credi, A., Venturi, M., Eds.; Wiley-VCH: Weinheim, Germany, 2008.

(4) Stoddart, J. F. *Acc. Chem. Res.* **2000**, *100*, 409.

(5) Erbas-Cakmak, S.; Leigh, D. A.; McTernan, C. T.; Nussbaumer, A. L. *Chem. Rev.* **2015**, *115*, 10081.

(6) Coskun, A.; Banaszak, M.; Astumian, R. D.; Stoddart, J. F.; Grzybowski, B. A. *Chem. Soc. Rev.* **2012**, *41*, 19.

(7) Kinbara, K.; Aida, T. *Chem. Rev.* **2005**, *105*, 1377.

(8) *Molecular Motors*; Schliwa, M. Wiley-VCH: Weinheim, Germany, 2003.

(9) *The Nature of the Mechanical Bond: From Molecules to Machines*; Bruns, C. J., Stoddart, J. F., Eds.; John Wiley and Sons: Hoboken, NJ, 2016.

(10) Kottas, G. S.; Clarke, L. I.; Horinek, D.; Michl, J. *Chem. Rev.* **2005**, *105*, 1281.

(11) Kassem, S.; van Leeuwen, T.; Lubbe, A. S.; Wilson, M. R.; Feringa, B. L.; Leigh, D. A. *Chem. Soc. Rev.* **2017**, *46*, 2592.

(12) Schoevaars, A. M.; Kruizinga, W.; Zijlstra, R. W. J.; Veldman, N.; Spek, A. L.; Feringa, B. L. *J. Org. Chem.* **1997**, *62*, 4943.

(13) Hiraoka, S.; Hisanaga, Y.; Shiro, M.; Shionoya, M. *Angew. Chem., Int. Ed.* **2010**, *49*, 1669.

(14) Vacek, J.; Michl, J. *Adv. Funct. Mater.* **2007**, *17*, 730.

(15) Michl, J.; Sykes, E. C. H. *ACS Nano* **2009**, *3*, 1042.

(16) Dominguez, Z.; Dang, H.; Strouse, M. J.; Garcia-Garibay, M. A. *J. Am. Chem. Soc.* **2002**, *124*, 2398.

(17) Lemouchi, C.; Iliopoulos, K.; Zorina, L.; Simonov, S.; Wzietek, P.; Cauchy, T.; Rodríguez-Fortea, A.; Canadell, E.; Kaleta, J.; Michl, J.; Gindre, D.; Chrysos, M.; Batail, P. *J. Am. Chem. Soc.* **2013**, *135*, 9366.

(18) Kelly, T. R.; De Silva, H.; Silva, R. A. *Nature* **1999**, *401*, 150.

(19) Bissell, R. A.; Cordova, E.; Kaifer, A. E.; Stoddart, J. F. *Nature* **1994**, *369*, 133.

(20) Hernandez, J. V.; Kay, E. R.; Leigh, D. A. *Science* **2004**, *306*, 1532.

(21) Koumura, N.; Zijlstra, R. W. J.; van Delden, R. A.; Harada, N.; Feringa, B. L. *Nature* **1999**, *401*, 152.

(22) Leigh, D. A.; Wong, J. K. Y.; Dehez, F.; Zerbetto, F. *Nature* **2003**, *424*, 174.

(23) Fletcher, S. P.; Dumur, F.; Pollard, M. M.; Feringa, B. L. *Science* **2005**, *310*, 80.

(24) Badjić, J. D.; Balzani, V.; Credi, A.; Silvi, S.; Stoddart, J. F. *Science* **2004**, *303*, 1845.

(25) Kassem, S.; Lee, A. T. L.; Leigh, D. A.; Markevicius, A.; Solà, J. *Nat. Chem.* **2016**, *8*, 138.

(26) Chen, J.; Wezenberg, S. J.; Feringa, B. L. *Chem. Commun.* **2016**, *52*, 6765.

(27) Kudernac, T.; Ruangsupapichat, N.; Parschau, M.; Macia, B.; Katsonis, N.; Harutyunyan, S. R.; Ernst, K. H.; Feringa, B. L. *Nature* **2011**, *479*, 208.

(28) von Delius, M.; Geertsema, E. M.; Leigh, D. A. *Nat. Chem.* **2010**, *2*, 96.

(29) Ragazzon, G.; Baroncini, M.; Silvi, S.; Venturi, M.; Credi, A. *Nat. Nanotechnol.* **2015**, *10*, 70.

(30) Lewandowski, B.; De Bo, G.; Ward, J. W.; Papmeyer, M.; Kuschel, S.; Aldegunde, M. J.; Gramlich, M. E.; Heckmann, D.; Goldup, M. S.; D'Souza, M. D.; Fernandes, A. E.; Leigh, D. *Science* **2013**, *339*, 189.

(31) *Molecular Devices and Machines - A Journey into the Nanoworld*; Balzani, V., Venturi, M., Credi, A., Eds.; Wiley-VCH: Weinheim, Germany, 2003.

(32) Pease, A. R.; Jeppesen, J. O.; Stoddart, J. F.; Luo, Y.; Collier, C. P.; Heath, J. R. *Acc. Chem. Res.* **2001**, *34*, 433.

DOI: 10.1021/jacs.7b05404
J. Am. Chem. Soc. 2017, 139, 10486−10498

(33) Qu, D. H.; Wang, Q. C.; Zhang, Q. W.; Ma, X.; Tian, H. *Chem. Rev.* **2015**, *115*, 7543.
(34) Klajn, R. *Chem. Soc. Rev.* **2014**, *43*, 148.
(35) Russew, M. M.; Hecht, S. *Adv. Mater.* **2010**, *22*, 3348.
(36) Balzani, V.; Credi, A.; Venturi, M. *ChemPhysChem* **2008**, *9*, 202.
(37) van Delden, R. A.; ter Wiel, M. K. J.; Pollard, M. M.; Vicario, J.; Koumura, N.; Feringa, B. L. *Nature* **2005**, *437*, 1337.
(38) Berná, J.; Leigh, D. A.; Lubomska, M.; Mendoza, S. M.; Pérez, E. M.; Rudolf, P.; Teobaldi, G.; Zerbetto, F. *Nat. Mater.* **2005**, *4*, 704.
(39) Tierney, H. L.; Murphy, C. J.; Jewell, A. D.; Baber, A. E.; Iski, E. V.; Khodaverdian, H. Y.; McGuire, A. F.; Klebanov, N.; Sykes, E. C. H. *Nat. Nanotechnol.* **2011**, *6*, 625.
(40) Zhu, K.; O'Keefe, C. A.; Vukotic, V. N.; Schurko, R. W.; Loeb, S. J. *Nat. Chem.* **2015**, *7*, 514.
(41) Deng, H.; Olson, M. A.; Stoddart, J. F.; Yaghi, O. M. *Nat. Chem.* **2010**, *2*, 439.
(42) Li, Q.; Fuks, G.; Moulin, E.; Maaloum, M.; Rawiso, M.; Kulic, I.; Foy, J. T.; Giuseppone, N. *Nat. Nanotechnol.* **2015**, *10*, 161.
(43) Natansohn, A.; Rochon, P. *Chem. Rev.* **2002**, *102*, 4139.
(44) van Oosten, C. L.; Bastiaansen, C. W. M.; Broer, D. J. *Nat. Mater.* **2009**, *8*, 677.
(45) Iamsaard, S.; Aßhoff, S. J.; Matt, B.; Kudernac, T.; Cornelissen, J. J. L. M.; Fletcher, S. P.; Katsonis, N. *Nat. Chem.* **2014**, *6*, 229.
(46) Eelkema, R.; Pollard, M. M.; Vicario, J.; Katsonis, N.; Ramon, B. S.; Bastiaansen, C. W. M.; Broer, D. J.; Feringa, B. L. *Nature* **2006**, *440*, 163.
(47) Kobr, L.; Zhao, K.; Shen, Y.; Comotti, A.; Bracco, S.; Shoemaker, R. K.; Sozzani, P.; Clark, N. A.; Price, J. C.; Rogers, C. T.; Michl, J. *J. Am. Chem. Soc.* **2012**, *134*, 10122.
(48) Zhao, K.; Dron, P. I.; Kaleta, J.; Rogers, C. T.; Michl, J. *Top. Curr. Chem.* **2014**, *354*, 163.
(49) Kaleta, J.; Dron, P. I.; Zhao, K.; Shen, Y.; Císařová, I.; Rogers, C. T.; Michl, J. *J. Org. Chem.* **2015**, *80*, 6173.
(50) Comotti, A.; Simonutti, R.; Catel, G.; Sozzani, P. *Chem. Mater.* **1999**, *11*, 1476.
(51) Brustolon, M.; Barbon, A.; Bortolus, M.; Maniero, A. L.; Sozzani, P.; Comotti, A.; Simonutti, R. *J. Am. Chem. Soc.* **2004**, *126*, 15512.
(52) Sozzani, P.; Comotti, A.; Bracco, S.; Simonutti, R. *Chem. Commun.* **2004**, 768.
(53) Bracco, S.; Comotti, A.; Ferretti, L.; Sozzani, P. *J. Am. Chem. Soc.* **2011**, *133*, 8982.
(54) Cipolloni, M.; Kaleta, J.; Mašát, M.; Dron, P. I.; Shen, Y.; Zhao, K.; Rogers, C. T.; Shoemaker, R. K.; Michl, J. *J. Phys. Chem. C* **2015**, *119*, 8805.
(55) Comotti, A.; Bracco, S.; Ferretti, L.; Mauri, M.; Simonutti, R.; Sozzani, P. *Chem. Commun.* **2007**, 350.
(56) Kaleta, J.; Kaletová, E.; Císařová, I.; Teat, S. J.; Michl, J. *J. Org. Chem.* **2015**, *80*, 10134.
(57) Vicario, J.; Walko, M.; Meetsma, A.; Feringa, B. L. *J. Am. Chem. Soc.* **2006**, *128*, 5127−5135.
(58) Chen, K. Y.; Wezenberg, S. J.; Carroll, G. T.; London, G.; Kistemaker, J. C. M.; Pijper, T. C.; Feringa, B. L. *J. Org. Chem.* **2014**, *79*, 7032.
(59) Comotti, A.; Simonutti, R.; Stramare, S.; Sozzani, P. *Nanotechnology* **1999**, *10*, 70.
(60) Allcock, H. R.; Levin, M. L.; Whittle, R. R. *Inorg. Chem.* **1986**, *25*, 41.
(61) Koumura, N.; Geertsema, E. M.; van Gelder, M. B.; Meetsma, A.; Feringa, B. L. *J. Am. Chem. Soc.* **2002**, *124*, 5037.
(62) ter Wiel, M. K. J.; van Delden, R. A.; Meetsma, A.; Feringa, B. L. *J. Am. Chem. Soc.* **2003**, *125*, 15076.
(63) Augulis, R.; Klok, M.; Feringa, B. L.; van Loosdrecht, P. H. M. *Phys. Status Solidi C* **2009**, *6*, 181.
(64) Conyard, J.; Addison, K.; Heisler, I. A.; Cnossen, A.; Browne, W. R.; Feringa, B. L.; Meech, S. R. *Nat. Chem.* **2012**, *4*, 547.
(65) Feringa, B. L.; Koumura, N.; Van Delden, R. A.; ter Wiel, M. K. J. *Appl. Phys. A: Mater. Sci. Process.* **2002**, *75*, 301.
(66) Klok, M.; Browne, W. R.; Feringa, B. L. *Phys. Chem. Chem. Phys.* **2009**, *11*, 9124.
(67) Vicario, J.; Meetsma, A.; Feringa, B. L. *Chem. Commun.* **2005**, 5910.
(68) Dron, P. I.; Zhao, K.; Kaleta, J.; Shen, Y.; Wen, J.; Shoemaker, R. K.; Rogers, C. T.; Michl, J. *Adv. Funct. Mater.* **2016**, *26*, 5718.
(69) Kaleta, J.; Nečas, M.; Mazal, C. *Eur. J. Org. Chem.* **2012**, *2012*, 4783.

DOI: 10.1021/jacs.7b05404
J. Am. Chem. Soc. 2017, 139, 10486−10498